Article

Unraveling Binding Effects of Cobalt(II)-Sepulchrate with the Monooxygenase P450BM-3 Heme Domain using Molecular Dynamics Simulations

Rajni Verma, Ulrich Schwaneberg, Dirk Holtmann, and Danilo Roccatano

Unraveling Binding Effects of Cobalt(II)Sepulchrate with the Monooxygenase P450BM-3 Heme Domain using Molecular Dynamics Simulations

Rajni Verma[c], Ulrich Schwaneberg[d], Dirk Holtmann[e], Danilo Roccatano[a,b,*]

[a] School of Mathematics and Physics, University of Lincoln, Brayford Pool, Lincoln, LN6 7TS, United Kingdom; [b]School of Engineering and Science, Jacobs University Bremen, Campus Ring 1, 28759 Bremen, Germany; [c]Department of Biomedical Engineering and Center for Biological Systems Engineering, Washington University in St. Louis, St. Louis, MO 63130; [d]Department of Biotechnology, RWTH Aachen University, Worringer Weg 1, 52074 Aachen, Germany; [e]DECHEMA-Forschungsinstitut, Biochemical Engineering Group, Theodor-Heuss-Allee 25, 60486 Frankfurt am Main, Germany.

*Corresponding author:

E-mail: droccatano@lincoln.ac.uk

Current Address: School of Mathematics and Physics, University of Lincoln, Brayford Pool, Lincoln, LN6 7TS, United Kingdom

ABSTRACT

One of the major limitations to exploit enzymes in industrial processes is their dependence on expensive reduction equivalents like NADPH to drive their catalytic cycle. Soluble electron transfer (ET) mediators like Cobalt(II)Sepulchrate have been proposed as a cost-effective alternative to shuttle electrons between an inexpensive electron source and enzyme redox center. The interactions of these molecules with enzymes are not elucidated at molecular level yet. Herein, molecular dynamics simulations are performed to understand the binding and ET mechanism of the Cobalt(II)Sepulchrate with the heme domain of cytochrome P450BM-3. The study provides a detailed map of ET mediator binding sites on protein surface that resulted prevalently composed by Asp and Glu amino acids. The Cobalt(II)Sepulchrate do not show a preferential binding to these sites. However, among the observed binding sites, only few of them provide efficient ET pathways to heme iron. The results of this study can be used to improve the ET mediator efficiency of the enzyme for possible biotechnological applications.

INTRODUCTION

Enzymatic electrocatalysis is a flourishing area of bioengineering with a plenty of applications in analytics, organic synthesis and diagnostics.[1-7] A class of enzymes that targets these applications is cytochrome P450 monooxygenases, a super family of heme-containing proteins.[8-14] In the presence of reduction equivalents, they catalyze the oxidation of substrates[12] involved in biosynthesis and biodegradation pathways, or in xenobiotic metabolism. The high stereoselectivity of these enzymes on a broad range of substrates is a treasure trove for potential industrial applications. However, their exploitation has been limited by their complex nature, low solubility and catalytic turnover and, in particular, the utilization of expensive electron source as nicotinamide adenine dinucleotide phosphate (NADPH).[12] Cytochrome P450BM-3, from soil bacterium *Bacillus megaterium,* is the most widely studied member of this family.[15-16] P450BM-3 has a high catalytic turnover with an easy expression and purification, being a soluble, multi-domain and self-sufficient system. One heme and two reductase domains (FAD domain and FMN domain, containing the flavin adenine dinucleotide and flavin mononucleotide molecule cofactors, respectively) are linked together as Heme-FMN-FAD in a single polypeptide chain.[17-19] The enzymatic reaction requires that two electrons be transferred from NADPH molecules to the heme iron by the two reductase domains. Protein engineering approaches successfully improved the technological viability of P450BM-3 by fine-tuning its catalytic parameters and substrate recognition.[20-21] Recently, fast advancements have been made toward cost effective catalysis in P450BM-3 by regeneration or substitution of expensive cofactor (NADPH/NADH) as a source of electrons.[13, 17] In last decades, electrochemistry of P450BM-3 received considerable attention and various methods have investigated to drive catalytic cycle either by direct contact with electrodes[22-23] or using molecules as electron transfer (ET) mediators. In the latter case, small

soluble compounds, such as cobalt(III)sepulchrate (Co(III)Sep), shuttle electrons from electrodes or other inexpensive electron sources (e.g. zinc dust) to enzyme redox site.[13, 24-25] However, little is known about the binding and ET mechanism of these mediators to the P450BM-3 at molecular level. To the best of our knowledge, only few experimental studies are devoted to identify the binding sites of ET mediators on the enzyme surface, which are relevant for ET mechanism in these systems. In particular, few mutagenesis studies have also been performed on the enzyme to obtain variants with improved mediated ET capabilities using directed evolution approaches.[24, 26] Strohle *et al*. proposed a computational method to identify suitable mediators for an artificial ET between an electrode and P450.[6, 27] Some of binding sites of the ET mediators were identified using conventional docking methods. Measured product formation rates could be qualitatively correlated with calculated ET rates providing a simple approach for the prediction of suitable mediators for P450s. However, this approach does not take in account the dynamics of the enzyme, the explicit solvent effects on the protein conformation and ET mediator binding.

Molecular dynamics (MD) simulation is so far the best theoretical approach to study at atomistic level both protein dynamics, and molecular binding mechanisms. MD simulations have been used to investigate the structure and dynamics of P450BM-3 heme[28-29] and FMN[30] domains in solution as isolated and in their complex.[31] In the last case, we have studied how the dynamics of FMN/heme complex affects the inter-domain ET rate.[31] These simulations evidenced an inter-domain conformational rearrangement that reduces the average distance between FMN and heme cofactors. The result was in agreement with the proposed hypothesis that the crystallographic FMN/heme complex is not in the optimal arrangement for favorable ET rate under physiological conditions.[19] ET rate calculations on the conformations sampled along the simulation, demonstrated the occurrence of seven ET pathways between two redox centers, while three of

them have ET rates (k_{ET}) comparable with experimentally observed values.[31] Collective modes analysis of FMN/heme complex also evidenced an interesting correlation between first two essential modes and ET pathways activation along the trajectory.

Here, we have combined MD docking simulations and ET calculations to garner insight into the interaction mechanism of P450BM-3 heme domain with Cobalt(II)sepulchrate (Co(II)Sep) as an ET mediator. We report a new model of Co(III/II)Sep based on GROMOS96 force field[32] parameters. The model was used for MD simulations of P450BM-3 heme domain in solution at different Co(II)Sep concentrations. The absorption of Co(II)Sep molecules on the heme domain surface provided a detailed map of its binding sites. Finally, the Co(II)Sep bound conformations of the protein were used to estimate using the Pathways method[33-34] the ET rates from Co(II) atom to the heme iron along different electron tunneling pathways.
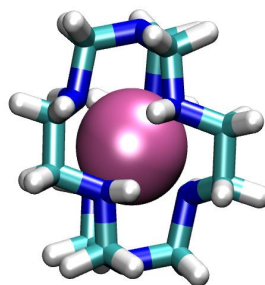
Figure 1: Crystallographic structure of the Co(III)Sep molecule in ball and stick representation. Nitrogen, hydrogen, carbon, and cobalt atoms are colored in blue, white, cyan and pink color, respectively.

COMPUTATIONAL METHODS

Co(III/II)Sep model. In Figure 1, the crystallographic structure of Co(III)Sep, obtained from Bacchi *et al.*[35], is represented. The force field parameters for bond lengths and bond angles of the Co(II)Sep model were adapted from Dehayes *et al.*[36] and they are reported in Table S1 of the Supporting Information (SI). Density functional theory (DFT) calculations[37-38] using Becke3LYP method[37] with the LanL2DZ basic set[38] were performed on both Co(II)Sep and Co(III)Sep molecules for geometry optimization. In the calculations, Co(III)Sep and Co(II)Sep have been considered in the experimental[39] observed low and high spin state, respectively. Atomic partial charges were derived using the ChelpG scheme[40] with dipole moment constraint, and they are reported in Table S2 of SI. All the calculations were performed using Gaussian09 package.[41]

The Lennard-Jones interaction parameters were taken from the GROMOS96 43a1 force field[32] library. The quality of models was assessed by comparing calculated self-diffusion coefficients (D) for Co(II/III)Sep with the experimental one.[14] The calculation of D were performed on three sets of 20 ns simulations started by assigning different initial velocities from Maxwell-Boltzmann velocity distributions at 300 K in a 3 nm cubic box of water (SPC model[42]) with a ET mediator molecule and Cl^- counter ions. The values of D obtained from Einstein relation[43] were $(0.84 \pm 0.01) \times 10^{-5}$ cm^2/s and $(0.98 \pm 0.07) \times 10^{-5}$ cm^2/s for Co(II)Sep and Co(III)Sep, respectively. By taking in account a rescaling factor ~1.7 due to the reduced viscosity of the SPC model with respect the experimental value of the water at the same temperature, the values reduce to 0.49 and 0.58×10^{-5} cm^2/s, respectively. For Co(III)Sep, the calculated value is within 15% of the available experimental value[14] of $(0.67 \pm 0.02) \times 10^{-5}$ cm^2/s.

Simulations setup. As starting crystallographic coordinates of heme domain (HEME) the chain A: 20 - 450) from the non-stoichiometric complex having one FMN domain and two heme domains (PDB ID: 1BVY, resolution of 0.2 nm).[44] In the starting conformation, the coordinates

of crystallographic water molecules within 0.60 nm from the HEME domain were also retained, while 1,2-ethanediol molecules were removed. The protonation state of protein residues was assumed to be the same as of corresponding isolated amino acids in solution at pH 7. GROMOS96 43a1 force field[32] used for all simulations was adopted for consistency with the previous simulation studies of the same enzyme.[45] Parameters of heme cofactor were the same as in our previous paper.[31]

The MD simulations were set up for HEME in water and aqueous Co(II)Sep solution at different Co(II)Sep concentrations. The simulation of isolated heme domain (150 ns) in water, used for the comparison, is an extension (up to 150 ns) of the one from our previous publication.[31] HEME was centered in a cubic periodic box of size ~9 nm. Co(II)Sep molecules were randomly placed in the simulation box. The simulations were performed at Co(II)Sep concentrations of 12.5 mM, 25.0 mM and 100.0 mM. We have used concentrations at least 2 times higher than those used in the available experimental studies (~5 mM)[13, 24] with the purpose to improve the sampling of protein binding sites using more Co(II)Sep molecules. At 12.5 mM Co(II)Sep concentration, three sets of simulations were performed starting with different conformations. These simulations though do not promise an exhaustive sampling of the protein surface at lower concentration, they still can provide a reliable mapping of the protein surface. Hence, the starting confirmation was solvated by stacking an equilibrated box of water molecules to fill the empty space in the simulation box. All the water molecules within 0.15 nm of another atoms were removed. SPC model[42] was used for the water molecules. Finally, chloride counter ions were added by replacing the solvent molecules at the most negative electrostatic potential to obtain a neutral system. These salt conditions have been used for consistency with previous simulations, however, we cannot exclude that the presence of higher concentration of buffering

salts as those used in experimental conditions may have an effect on the CoSep binding. We are

planning to explore this aspect in future simulations of the enzyme. Compositions of all

simulated systems are summarized in Table 1.

Table 1: Simulation summary of P450BM-3 HEME in water and aqueous Co(II)Sep solution.

Simulation name	No. of atoms	No. of Co(II)Sep	Co(II)Sep conc. (mM)	No. of solvent molecules	No. of counter ions	Set of simulations
WAT	65650	-	00.0	20365	16 Na$^+$	1
5CoS(I-III)	65550	5	12.5	20290	6 Na$^+$	3
10CoS	65434	10	25.0	20207	4 Cl$^-$	1
40CoS	64597	40	100.0	19638	64 Cl$^-$	1

Molecular dynamics simulation protocol. The LINCS[46] algorithm was used to constrain

all bond lengths and SETTLE[47] algorithm was used for water molecules. Electrostatic

interactions were calculated using Particle Mesh Ewalds method.[48] For the calculation of long-

range interactions, a grid spacing of 0.12 nm, combined with a fourth-order B-spline

interpolation were used to compute the potential and forces between grid points. A non-bonded

pair-list cutoff of 1.3 nm was used and updated at every 5 time-steps. Berendsen's thermostat[49]

was used to keep temperature at 300 K by weak coupling system to an external thermal bath with

a relaxation time constant τ = 0.1 ps. Pressure of the system was kept at 1 bar by using

Berendsen's barostat[49] with a time constant of 1 ps.

The systems were first energy minimized for at least 2000 steps using steepest descent

method to remove possible clashes between atoms. After energy minimization, all atoms were

given an initial velocity obtained from a Maxwellian distribution at 300 K. A time step of 2 fs

was used to integrate the equation of motions. First, the system was equilibrated for 100 ps by applying position restraints to the heavy atoms for solvent equilibration. Hence, position restraints were removed and the systems were gradually heated up from 50 K to 300 K during 200 ps simulation. Finally, production runs of 150 ns were performed for all simulations at 300 K. The GROMACS software package was used to run MD simulations and analysis of trajectories.[50] VMD 1.9.1[51] and UCSF Chimera[52] molecular visualization packages were used for figure preparation. The crystal structure of HEME was used as reference for the analysis of trajectories.

Cluster analysis. Cluster analysis was performed to characterize conformational diversity of protein conformations selected for ET pathway analysis. The Gromos clustering algorithm[53] was used for the cluster analysis. The clustering method is based on the analysis of the root-mean square deviation (RMSD) matrix of a set of atoms from selected conformations along the simulation.[53] A structure is assigned to a cluster if its RMSD from the cluster median structure is within a given cutoff. In this work, the method was applied to the backbone atoms and a RMSD cutoff of 0.11 nm was used.

Electron transfer tunneling. ET tunneling from Co(II) atoms to heme iron was calculated using Pathways program.[33, 54] The model for the ET transfer calculation, as implemented in Pathways, gives an approximate description of electronic coupling matrix and rate constants since it is based on empirical approximations.

For a given protein conformation, the program identifies an effective ET coupling by evaluating the highest electronic tunneling coupling (T_{DA}) through different pathways connecting donor and acceptor through bonds and space.[33] In particular, the program identify a series of consecutive inter-atomic distances from a given electron donor to acceptor, and whether the

electron travel along each of them via a covalent bond (*cb*), hydrogen bond (*hb*) or through space

jump (*sj*), contribution (ε) to the pathway T_{DA} are calculated using following empirical

expressions:

$$\varepsilon_i^{cb} = 0.60 \tag{1}$$

$$\tag{2}$$

$$\varepsilon_j^{hb} = 0.36e^{-1.70(R-2.80)}$$

$$\varepsilon_k^{sj} = 0.60e^{-1.70(R-1.40)} \tag{3}$$

where R (in Ångstrom) is the distance between two atoms in a path segment. Hence, T_{DA} value is

calculated as proportional to the product of all contributions along the electron pathway:

$$T_{DA} \alpha \prod_i \varepsilon_i^{cb} \prod_j \varepsilon_j^{hb} \prod_k \varepsilon_k^{sj} \tag{4}$$

Finally, a non-adiabatic ET reaction rate (k_{ET}) for a given pathway was estimated using following

equation:[55]

$$k_{ET} = \frac{2\pi}{\hbar} \frac{\exp\left[-(\Delta G + \lambda)^2 / 4\lambda k_B T\right]}{\sqrt{4\pi\lambda k_B T}} |T_{DA}|^2 \tag{5}$$

where ΔG is driving force and λ is Marcus reorganization energy for the ET reaction, $\hbar = h/2\pi$

with Plank constant, h, and k_B is Boltzmann constant. Difference in the reduction potential of

Co(II)Sep and heme cofactor (0.188 eV) was used as a value for ΔG.[19, 26, 56-57] λ is equal to 0.7

eV as a good approximation for ET in a system with more than 1.0 nm distance between donor to acceptor.[57-58] Characteristic ET pathways and the average values of T_{DA} and k_{ET} were calculated from 25 conformations extracted in 2 ns intervals over the last 50 ns simulations. The 2D graphs of the pathways were generated using the *graphviz* software (http://www.graphviz.org).

ET mediator binding energy. The binding energies of the Co(II)Sep molecules to the enzyme was estimated in each simulation by calculating their averaged non-bonding interactions (electrostatics and van der Waals) with the rest of the system in their bound and unbound state. A Co(II)Sep molecule was considered bound to the protein if its minimum distance from the protein surface amino acids was less then 0.4 nm. The binding energy was thus calculated from the averaged energy of bounded and unbounded ET mediator states as $\Delta E = <E_{bound}> - <E_{unbound}>$.

RESULTS AND DISCUSSIONS

General Structural and Dynamics Properties. In Table 2 and Figure S1 of SI, backbone-backbone root mean square deviation (RMSD) curves and their average values calculated on last 50 ns simulations are reported, respectively. The values indicates a possible effect of Co(II)Sep concentration on the protein structure and dynamics. At 0 mM and 12.5 mM Co(II)Sep concentrations, RMSD curves deviate the most from the crystal structure and stabilize to a average value of ~0.33 nm. At 25 mM Co(II)Sep, the curve shows plateau after 110 ns simulation to an average value of 0.31 ± 0.01 nm. The lowest RMSD value was observed for 100 mM Co(II)Sep conc., where RMSD curve leveled to the constant value of ~0.25 nm after 50 ns of simulation. Average values of both radius of gyration (Rg) and surface accessible area (SASA), in Table 2 show small differences in CoSep-water simulations (even at high Co(II)Sep

concentrations) that suggests the slight effect of ET mediator on the compactness and overall stability of HEME.

Table 2: Average values of the backbone RMSD, RMSF, Rg, and total (T), hydrophobic (Ho) and hydrophilic (Hi) SASA calculated from the last 50 ns of each simulation.

	WAT	5CoS(I)	5CoS(II)	5CoS(III)	10CoS	40CoS
RMSD	0.35±0.01	0.36±0.01	0.31±0.01	0.34±0.01	0.31±0.01	0.25±0.01
RMSF	0.08±0.03	0.09±0.09	0.09±0.06	0.10±0.05	0.08±0.04	0.07±0.03
Rg	2.13±0.01	2.14±0.01	2.11±0.01	2.11±0.01	2.13±0.01	2.14±0.01
Ho.SASA	101±2	102±2	104±2	103±2	106±2	102±2
Hi.SASA	90±2	93±2	93±2	94±2	95±2	97±2
T. SASA	192±3	195±3	198±3	197±3	200±3	198±3

The average conformation variations of HEME were analyzed using RMSD per residue (bottom panel in Figure 2). At higher Co(II)Sep concentrations (at 25 mM and, in particular, at 100 mM Co(II)Sep conc.), HEME shows smaller deviations from the crystallographic structure than the one observed in simulations at 12.5 mM concentration. In particular, significant differences between the highest and lowest Co(II)Sep concentrations were observed only in correspondence to E/F, F/G and G/H loop regions.

In Figure 2 (top panel), the root mean square fluctuations (RMSF) per residue are reported. The curves follow the trend observed for the RMSD per residue curves. As expected from previous simulation studies of P450BM-3,[28-29, 31] the highest mobility was observed in the

loop regions. The presence of Co(II)Sep slightly increased the RMSFs in correspondence of A
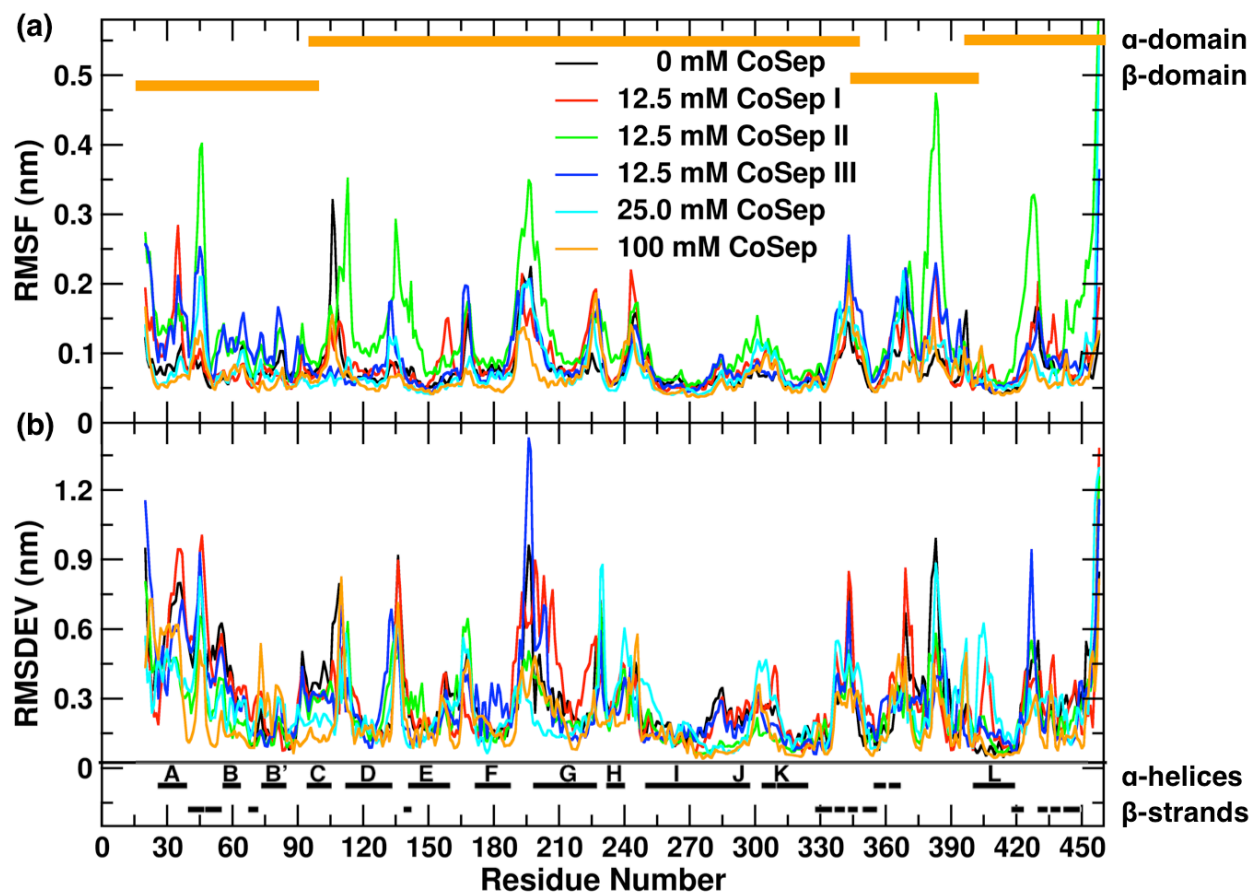
helix and A/B, C/D, F/G and K/L loop regions.

Figure 2: Backbone RMSD (bottom panel) and RMSF (top panel) per residue with respect to crystal

structure for HEME at 0.0, 12.5, 25.0 and 100 mM Co(II)Sep, respectively. Horizontal bars represent

helices and β-strands locations at the bottom panel (in black color), and two structural subdomains of

HEME at the top panel (in orange color).

A relevant aspect of HEME structure is the accessibility of its active site that is regulated

by the opening of substrate access channel (SAC). SAC opening can be monitored by distance

between Cα of Pro45 and Ala191 residues that is equal to 1.61 nm in the starting

crystallographic structure.[59] Time series of the latter distances are reported in Figure S2 of SI for all simulations.[28, 30] The protein remains in the open conformation with an average distance of 1.19 ± 0.09 nm calculated in the last 10 ns of water simulation. This value is in agreement with the result from our previous study.[28, 30] During the 12.5 mM Co(II)Sep conc. simulation, the SAC opening fluctuates between the open and close states until it adopts the close one (average distance of 0.58 ± 0.05 nm) at the end of the simulation. Moreover, the increase of Co(II)Sep concentration tends to stabilize SAC opening state with P45Cα-A191Cα distance comparable of or even higher than the one observed in the crystallographic structure. Interestingly, previous MD simulation studies of the HEME domain in 14% (v/v) DMSO/water mixtures[28-29] have also showed the tendency of the protein to adopt the open conformation.

CoSep binding to the HEME surface. Co(II)Sep binding to the HEME was monitored by counting the number of contacts between ions and protein within a cutoff distance of 0.6 nm. The Co(II)Sep molecules diffuse and bind to the HEME in the first 10-25 ns of simulations. In the last 50 ns of the 5CoS (I, II, III), 10CoS and 40CoS simulations, 4, 8 and 37 Co(II)Sep molecules, respectively, steadily bound to the HEME surface with an average distance of 0.17 ± 0.01 nm. Figure 3 shows Co(II)Sep molecules absorbed on HEME surface at the end of 5CoS II (A), 10CoS (B) and 40CoS (C) simulations.

The amino acid composition of the HEME surface was calculated by counting all residues with the solvent accessible surface area, averaged in the last 50 ns of the simulation, larger than 0.35 nm^2. In Table S3 of SI, the surface amino acids composition for each simulation are reported as the number of hydrophobic, charged, polar, aromatic and glycine amino acids. The trend is similar for all the simulations. The negatively charged Asp is the most abundant amino acid (~26%), followed by positively charged (22-23%, mainly Lys), polar (22%),

hydrophobic (~18%), aromatics (~7%) and Gly (3-4%). Number of amino acid types having more than 6 contacts with Co(II)Sep molecules are reported in Table S4 for each simulation. Co(II)Sep binding sites, as expected from being positively charged, are prevalently bound to negatively charged (31-49%) and polar (21-27%) amino acids.

In Figure S4 of SI, time series of contact occurrences between Co(II)Sep molecules and HEME residues in the last 50 ns of the simulations are reported. Only the residues with a percentage number of contact occurrence along the trajectory larger than 80% are reported. In all these cases, Co(II)Sep molecules bind very steadily to the protein with few and short unbinding events.

A total number of 130 surface residues, corresponding to ~63 % of the total surface amino acids (206), are involved in the binding in all the simulations. The simulations 5CoS(I+II+III), 10CoS and 40CoS accounts for 41, 29 and 108 amino acids respectively. These common amino acids are 10, 23 and 26 for the pairs 5CoS-10CoS, 5CoS-40CoS and 10CoS-40CoS, respectively. In 40CoS simulation, most of the negatively charged and polar residues on HEME surface are occupied by Co(II)Sep molecules providing an extensive list of binding sites on protein surface. As shown in previous section, our study suggests that Co(II)Sep concentrations also influence the extend of SAC opening (Figure S2 of SI). However, despite the widening of the SAC entrance in the simulations at the highest Co(II)Sep concentration, none of the Co(II)Sep molecule was able to diffuse inside the protein. It is possible that the positive charged residues in the proximity of entrance and inside SAC (as the Arg47) can indeed impede to positive ions the access into the SAC. However, a recently solved crystallographic structure of a P450BM-3 multivariant with also Arg47→Phe47, obtained from protein crystals soaked in 5

mM Co(III)Sep solution, do not show the presence of ET mediator molecules in the active site
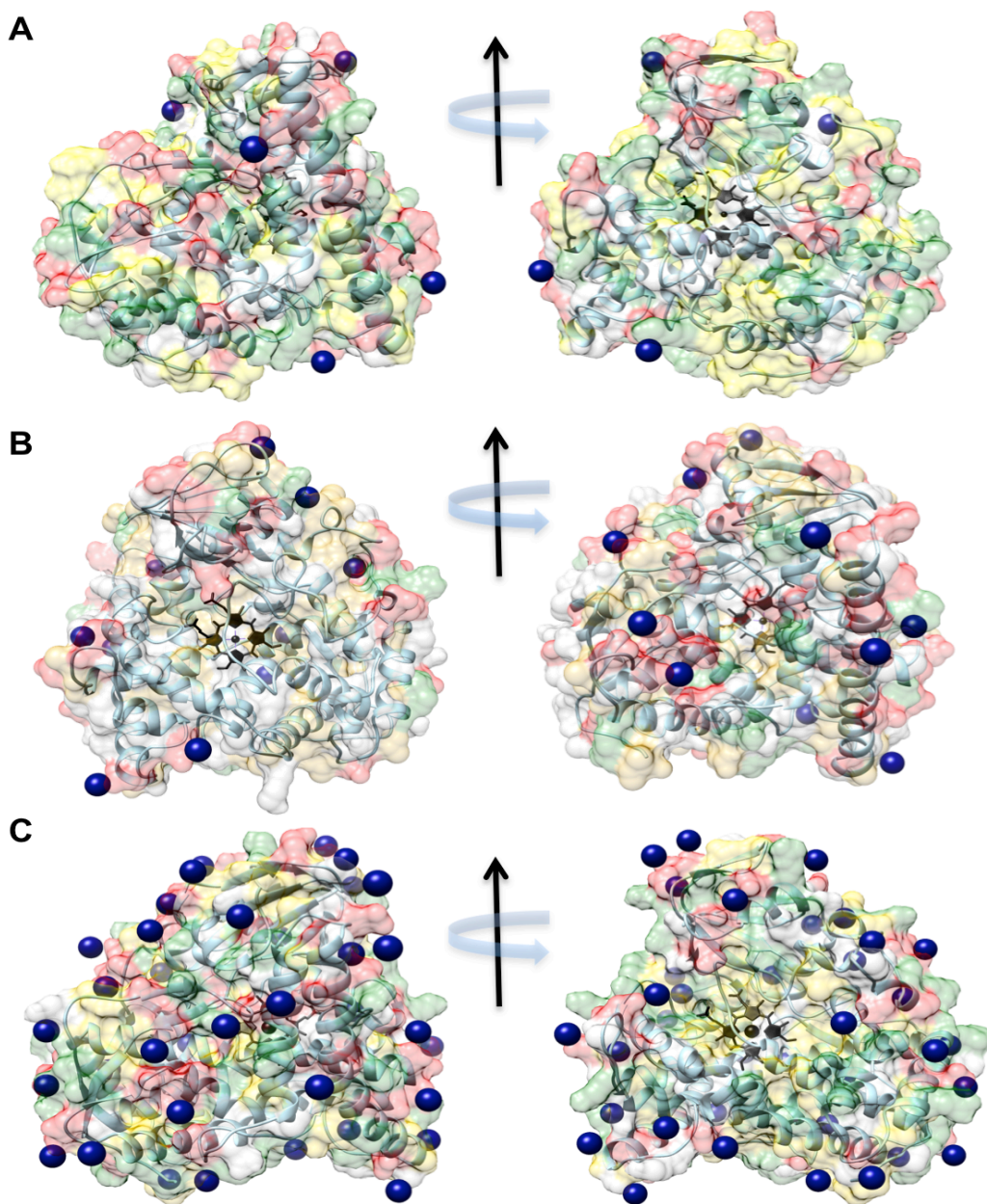
pocket .[60]

Figure 3: Co(II)Sep binding on HEME is in the last frame of 150 ns simulation of water-Co(II)Sep

solutions at a conc. of 12.5 mM (A), 25.0 mM (B) and 100 mM (C). Co atom of Co(II)Sep molecules is

in blue colored vdw representation. HEME is in cartoon representation (sky blue) with surface colored by

charged residue type (positive charge in green and negative charge in red color) and hydrophobic residues (in yellow color). Heme cofactor is in black colored licorice representation.

ET tunneling of Co(II)Sep to the Heme. ET tunneling and rate constants have been estimated using 25 conformations, sampled every 2 ns in the last 50 ns of each simulation. The structural differences in the conformers were analyzed using cluster analysis (see Methods) using a combined trajectory of 150 conformations from all simulations. In Figure S3 of SI, backbone RMSD matrix calculated on the combined trajectory is reported. RMSD values are up to 0.16 nm within each simulation, and larger than 0.3 nm among the six simulations evidencing in this case a large conformational diversity.

Table 3: **Number of bound Co(II)Sep molecules in each simulation grouped by calculated k_{ET} value, and statistics of different amino acid types involved in Co(II)Sep binding.**

	5CoS (I)	5CoS (II)	5CoS (III)	10CoS		40CoS	
k_{ET} (s^{-1})		<10		<10	≥10	<10	≥10
No. Co(II)Sep	4	3	3	8	2	28	11
Hydrophobic	1	0	0	3	1	7	2
Polar	6	4	0	8	4	25	6
Positive charged	0	1	0	3	0	8	2
Negative charged	6	5	5	13	1	40	6
Glycine	0	1	0	0	0	2	0
Aromatic	0	0	0	1	0	6	1

Total bound Amino acids	12	11	5	28	6	88	17

The largest deviations occur between the conformations from WAT, 5CoS and 10CoS simulations. Cluster analysis on the combined trajectory gives 61 clusters, which are mainly localized within each simulation, as shown in the lower triangular part of RMSD matrix in Figure S3 of SI.

The 25 conformations were used to perform the calculation of the ET pathways as described in the Methods section. The pathway analysis gives a total of 112 surface residues involved ET pathways. In Table 3, amino acid type statistics of Co(II)Sep binding sites is reported. As expected, the bonding sites of Co(II)Sep in all the pathways are prevalently negatively charged or polar. Since accurate experimental measurements of k_{ET} for this system are not available, we grouped ET pathways based on calculated k_{ET} values as low rate ($k_{ET} < 10$ s^{-1}) or high rate ($k_{ET} \geq 10$ s^{-1}) for a qualitatively assessment. Half of these amino acids are involved in pathways with $k_{ET} \geq 0.1$ s^{-1} and they are reported in Table 5S. From 5CoS simulations only pathways yielding $k_{ET} < 10$ s^{-1} have been observed. For the other simulations, 35% of Co(II)Sep binding sites (18) are wired to the heme iron through pathways yielding $k_{ET} \geq 10$ s^{-1}.

The eighteen amino acids involved in pathways with $k_{ET} \geq 10$ s^{-1} are reported in Table 4. These residues are the part of B, C and I helices, and B/B', B'/C, C/D and H/I loops. Among these, H100, P105, E244, H388 and N397 amino acids are also localized at FMN/HEME interface as in the crystal structure (PDB-ID: 1BVY), and from our recent simulation study of HEME/FMN complex.[31] The other binding site residues are observed on distal side of HEME in proximity of near the SAC.

Table 4: List of HEME residues involved in Co(II)Sep binding and in the pathways of ET rates ≥ 10 s^{-1}. Third column reports secondary structure element in which amino acids is located. The fourth column report the maximum value of k_{ET} observed for the Co(II)Sep bound to this residue. Amino acids located in correspondence of HEME/FMN domain interface are indicated with 'X' in column 5. Columns 6-10 indicate Co(II)Sep binding to HEME residues. Last column indicates amino acid mutation(s) reported in literature for HEME residues involved in Co(II)Sep binding.

N.	Res. No.	Res. Name	Secondary Structure	k_{ET} (s^{-1})	Heme/ FMN Interf.	5Co S (II)	10C oS	40CoS	Reported mutations
1	23	ASP	coil-loop: lc1	174.8				30, 35, 38	
2	63	ASP	coil-loop: lc5	10.8				19	
3	71	LEU	coil-loop: lc6	406.1				10	
4	76	LYS	α-helix: B'	971.8				10	SER[61-62]
5	80	ASP	α-helix: B'	1146.3				10	PRO[61-62]
6	84	ASP	coil-loop: lc7	1706.5			1	6	THR[61-62]
7	95	ASN	α-helix: C	3027.6			1		
8	96	TRP	α-helix: C	398.3				5	ALA/PHE/TYR[63-65]
9	100	HIS	α-helix: C	34950.4	X			5	ARG[66-67]
10	105	PRO	3_{10}-helix: a	470.2	X		5		
11	106	SER	3_{10}-helix: a	46.9			5	12	ARG[67]
12	244	GLU	coil-loop: lc13	297.3	X			5, 8	
13	253	ASN	α-helix: I	259.6			1	6	
14	351	ASP	coil-loop: lc20	27.7		1	6	14, 35	
15	359	GLN	α-helix: K'	156.3		3			
16	388	HIS	coil-loop: lc22	468.6	X			19	
17	397	GLN	Cys-pocket: p1	1321.9	X			5	
18	440	LYS	β-sheet: 4.2	31.3				29	ASN[68]

In Figure 4A, Co(II)Sep binding residues, listed in Table 5S, are represented as van der Walls (VdW) sphere on the crystal structure of FMN/HEME complex.[44] Figure 4B is the same representation of the protein with the binding residues involved in pathways colored according to the k_{ET} values. The distribution of Co(II)Sep binding sites on the protein surface follows the surface electrostatic properties. However, only few binding residues act as electron acceptors for ET to heme iron, and they are localized in specific locations as in proximity of the SAC and at the FMN/HEME interface. Interestingly, the last one has been optimized by the nature to enhance the ET between reductase and HEME domains.
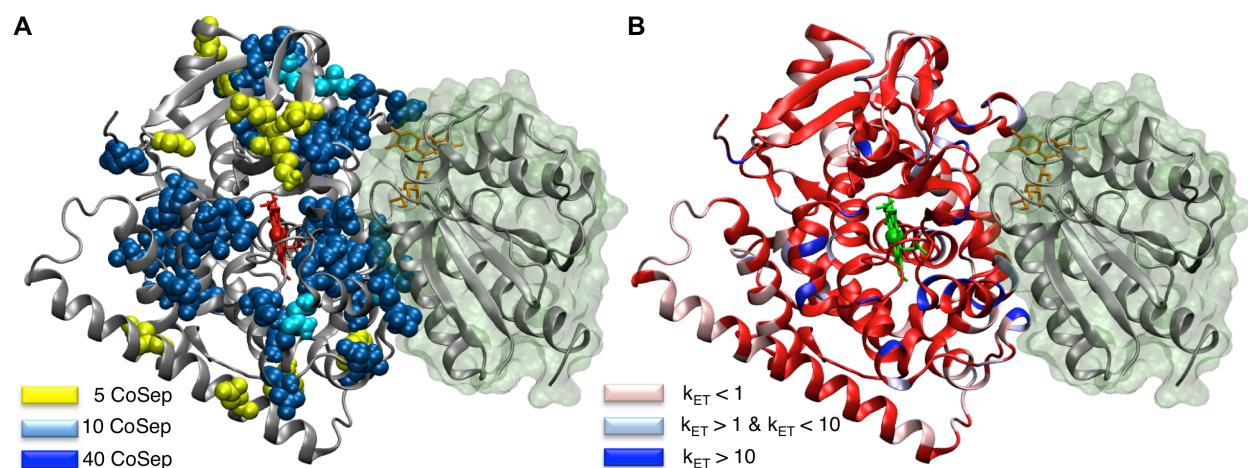

Figure 4: HEME/FMN complex is in cartoon representation colored by gray color. Heme cofactor is in red (A) and green (B) colors, and FMN cofactor is in orange colored licorice representation. FMN domain has green color surface representation. **(A)** Co(II)Sep binding residues are in VdW representation colored by yellow, cyan and blue for 5CoS, 10CoS and 40CoS simulations, respectively. **(B)** Residues involved in ET pathways with $k_{ET} < 1$, $1 < k_{ET} < 10$, and $k_{ET} \geq 10$ are in cartoon representation colored by pink, ice blue and blue color, respectively.

The pathways formed by cluster of residues from the selected Co(II)Sep molecules are partially interconnected and forming a network. In Figure 5 and S6, the combined ET pathways network obtained from all the simulations are reported. In order to simplify the visualization, the network of Figure 5 shows only the pathways with $k_{ET} \geq 10$ s^{-1} and occurring in the analyzed conformations more than 5 times. The number of bonded Co(II)Sep molecules are in total three, two and six from the 5CoS(II), 10CoS and 40CoS simulations, respectively. For $k_{ET} \geq 10$ s^{-1}, this number reduces to 9 since only one pathway 5CoS simulation fulfills this condition.

The different pathways are represented in different colors and the line thickness is proportional to the number of protein conformations in which the same pathway was observed. In Table S5, S6 and S6 of SI, these pathways are listed with their average k_{ET} values and occurrences in the selected conformations in the different simulations. The graph clearly shows that most of the Co(II)Sep molecules docked to gateway residues for 7 preferential pathways (tick lines). Beside the residues present in these main pathways, there are several other ones involved in the formation of transient and secondary ET lanes along the main routes (see Figure S5). In addition, although in a less extended, interconnectivity among principal pathways from different Co(II)Sep molecules is also observed (see Figure S5). The main pathways comprise from 1 to 6 intermediate amino acids (in the extended graph of Figure 5S, pathways can comprise up to 8 amino acids). The pathways amino acids composition is 20% hydrophobic, 40% polar, 20% charged, 10% glycine and 10% aromatics, with the charged residues as binding residues as mentioned before.

These networks reflect the local structural organization of the residues involved. In Figure 6, as representative examples, residues involved in the ET for the last simulation conformation from the 10CoS and 40CoS simulations are shown. For the 10CoSep simulation, two preferential

pathways have starting from Asp84 (Co1_10) and Ser106 (Co5_10) residues (see Figure 5) are present. As shown in Figure6A, they comprise 3 and 4 amino acids, respectively located in B'/C loop (D84, G85 and A86), helix C (S106 and F107), and K/L loop (I401 and C400). The pathways starting from Co5_10 are located in proximity of the FMN/HEME binding interface of the complex, the other one on the opposite side (see Figure 4 and 6A).

In the 40CoSep simulation, six dominant pathways, with two in common with the 5CoS(II) and 10CoS simulations (see Figure 6B) respectively, have been observed. The pathways start from two His residues (100 and 388), three Asp (84, 351 and 23), Ser106 and Lys76. The shorter pathway (from Co5) comprises the His100 only, while the longer one from Co19 5 and from Co14 6 residues, respectively. These pathways involve residues of N-terminus (D23), helix B' (Q73 and K76), and B/B' (S72), B'C (D84, G85 and A86), K/L (L333, S332, D351, E352, L353, H388, F393, G394, N395, C400) loops. As shown in Figure 6B, two pathways (from Co19 and Co5) have residues facing the FMN/HEME interface region (see Figure 4) while the other are more distant with two of them near to the SAC entrance (Co38, Co10). Interestingly, the binding site of Co14 is common to the one of Co1 in the 5CoS(II) simulation.

The average binding energies (ΔE) of each Co(II)Sep in the last 50 ns of each simulation is reported in Table7S of SI. For the 5CoS(II) simulation, three Co(II)Sep molecules involved in ET with $k_{ET} > 10$ s^{-1} have values of -68 (Co1, Co4) and -119 (Co3) kJ/mol. The Co3 molecule has the lowest energy among all the binding molecules but its pathways is a transient one occurring less than 6 time in the 25 sampled conformations. The more stable Co1 share the same pathway with the Co14 in the 40CoS simulation. The last one has a binding energy of -77 kJ/mol that it is close to the value of the Co1 in 5CoS simulation. For the 10CoS simulation, the two Co(II)Sep molecules involved in the ET have value of ΔE of -80 (Co1) and -73 (Co5) kJ/mol,

respectively. These values are higher than the average one of -85.9 kJ/mol. The Co1 molecule

share the same pathway of the Co6 one in the 40CoS simulation that it has also a very similar ΔE

value (**-**79 kJ/mol). Finally, for the 40CoS simulation, the six Co(II)Sep involved have ΔE values

equal to -74, -79, -74, -77, -87, -81 kJ/mol that are lower than the average (-70.8 kJ/mol) but not

the lowest ones (see Table 7Sb) among the binding molecules.

Overall these results indicate a poor discrimination of the Co(II0Sep for the different

binding sites of the enzyme and a lack of correlations between the best binding energy and the

most efficient pathways k_{ET}. Several amino acids, which are involved in the observed ET

pathways, are also targeted in mutagenesis experiments of P450 BM-3 (for a complete and recent
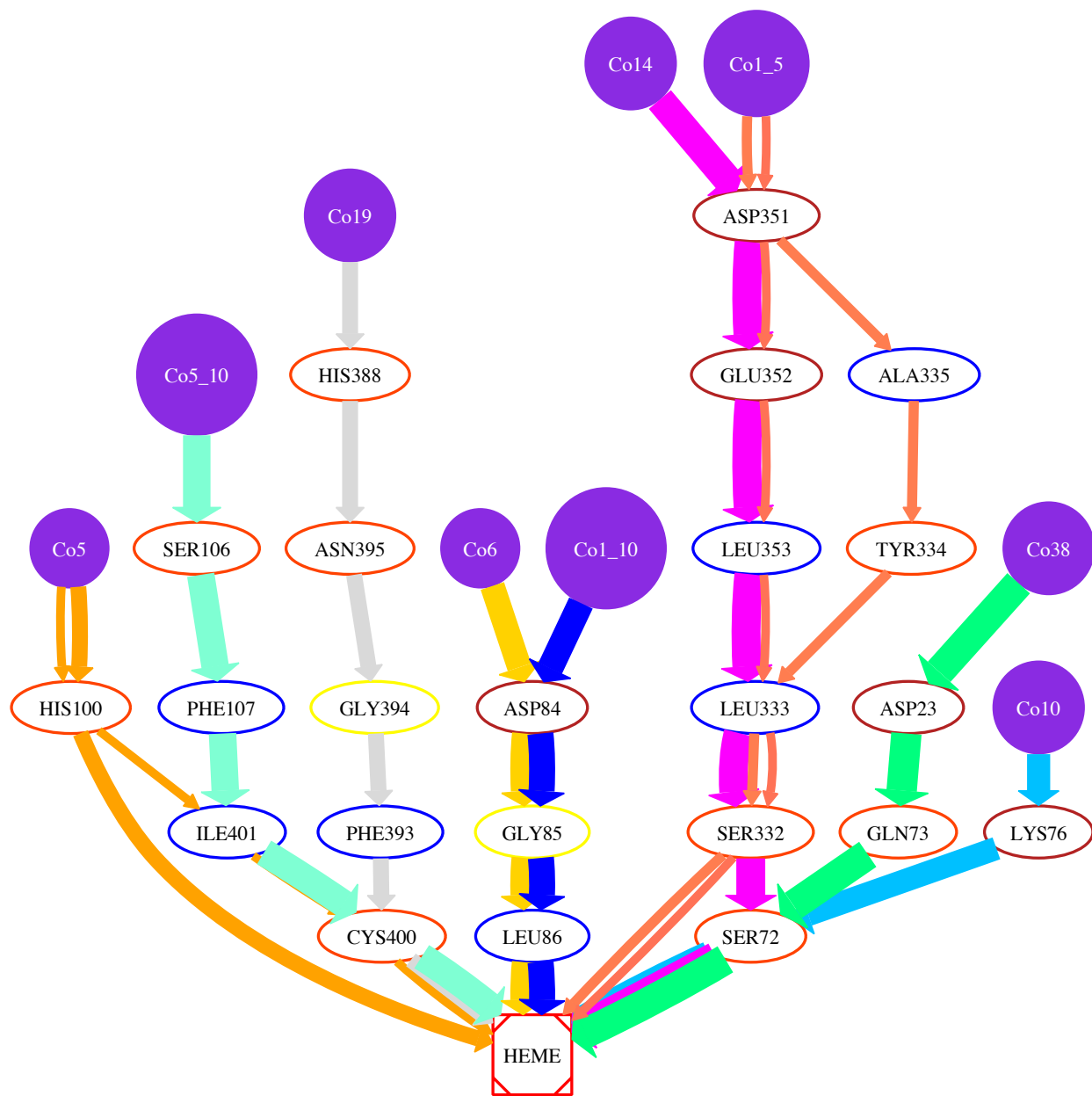
list of P450 BM-3 mutants see Ref.[17]).

Figure 5: Combined representation of ET pathways with $k_{ET} \geq 10$ s^{-1} and occurring more then 25% of the analyzed conformations from 5CoS, 10CoS and 40CoS simulation. The pathways are indicated using separate colors. The line thickness represents the number of conformations in which the pathway was observed. The color of ellipse around the amino acids names reflects the chemical nature of the amino acid (red: polar, brown: charged, blue: hydrophobic and aromatic; yellow: glycine).

Experimental mutagenesis studies at the HEME binding positions of Co(II)Sep observed in this study are indicated in the last column of Table 4 and Table 5S of SI. To the best of our knowledge, only one experimental study on the activity of P450 BM-3 wild-type and mutants, with improved activity with respect WT P450 BM-3, has been reported in the literature for this system.[24] The improved HEME mutant, obtained by directed mutagenesis methods, contains the following substitutions F87A, R47F, V281G, M354S, D363H. Interestingly, the mutation D363H (see Table 4 and Table S5) coincides with one of the identified residues involved in low rate ET pathway ($k_{ET} < 1$). However, considering the large number of mutations, it is difficult to make any conclusion on its role on the enhanced enzymatic activity of this mutant.
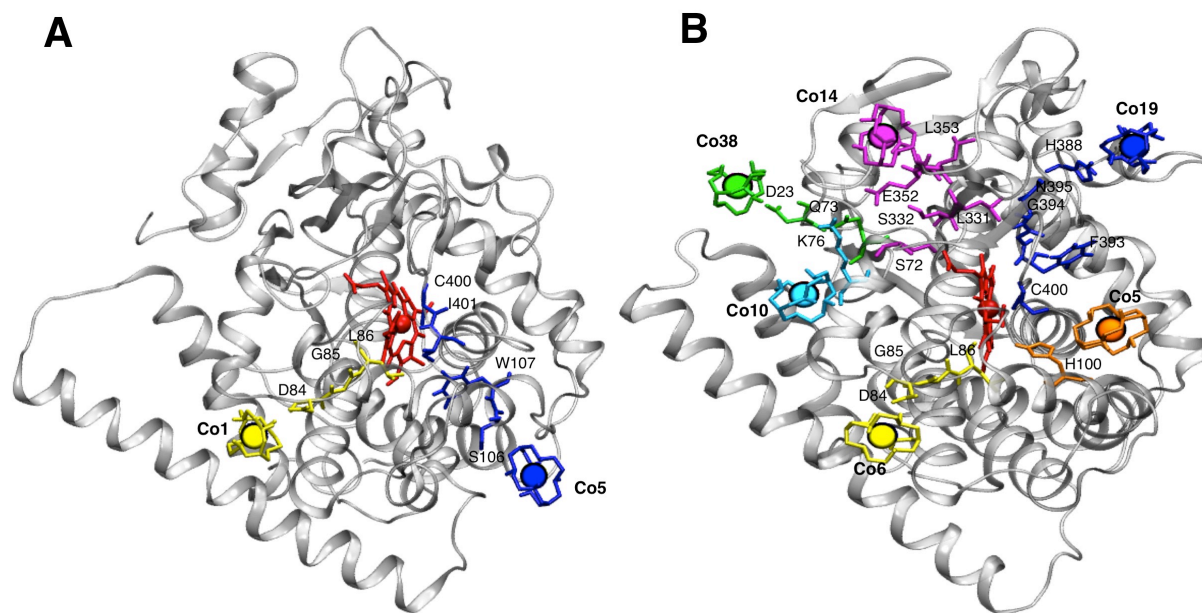

Figure 6: HEME conformation is in cartoon representation using the last frame of (A) 10CoS and (B) 40CoS 150ns simulations. Cobalt and iron atoms are shown in VdW representation. Heme cofactor and residues involved in the main ET pathways in Figure 5 are represented as colored sticks.

CONCLUSIONS

A MD simulations study of P450 BM-3 heme domain has been performed in aqueous solution of ET mediator cobalt(II)sepulchrate at three different concentrations. The results of simulations illustrate the absorption mechanism of ET mediator on protein surface at molecular level, its effect on enzyme structure and dynamics, and possible ET pathways from binding site to heme iron.

Although P450 domain structure does not change significantly from the crystallographic starting one, a dependence of protein conformational variations on the Co(II)Sep concentration was observed. In particular, at high Co(II)Sep concentrations, the protein has a reduced backbone fluctuations as a consequence of large number of Co(II)Sep ions absorbed on its surface. In addition, high Co(II)Sep concentrations tend to open of substrate access channel with possible effects on the enzymatic activity. Co(II)Sep ions typically bind on the exposed loop regions of the protein surface (containing more negatively charged amino acids) reducing their flexibility. Unfortunately, experimental structural studies of the protein at high Co(II)Sep concentration are not yet available. However, it would be interesting to experimentally verify the effect of the ET mediators on the structural and dynamics properties of the enzyme.

The results also showed that Co(II)Sep ions tend to be absorbed rapidly by the protein surface and remain bounded to it. This suggests that the oxidized form Co(III) of the mediator, having a stronger electrostatic affinity with negative amino acids than the reduced one, can more strongly bound and, eventually, saturate all the binding sites of the protein surface. In this conditions the reduction of Co(III)Sep ions might take place either directly by electron source (e.g. zinc dust) or indirectly by other reduced electron mediators present in solution.

Only 25-28% of identified Co(II)Sep binding sites are connected to heme iron with ET pathways yielding ET rates $k_{ET} \geq 10$ s^{-1}. This percentage drops even more if constraints on frequency of pathway occurrence in the analyses conformation are introduced. Some of these sites are located in regions proximal to interface with FMN domain as from the crystallographic structure of FMN/HEME complex. However, other high ET rate pathways have been identified starting from regions closed to SAC region. The analysis of the binding energy reveals poor binding specificity and no correlation with the calculated ET rate. This is not surprising since the heme domain of P450BM-3 structure is not naturally evolved to efficiently drive its catalysis using small ET mediators as electron source.

In order to achieve a high productivity in electro-enzymatic processes, ET from mediator to enzyme redox center is one of the most important parameters to achieve the overall goal of high product formation.[69] Mutations at the amino acids positions involved in calculated ET pathways are reported in the literature, but only very few of these mutants have been studied in the presence of Co(II)Sep. The results of our study show that there are few amino acids that are potential binding sites that can have also favorable ET pathways. Unfortunately, there are not experimental data on the kinetics of ET between Co(II)Sep and heme domain. However, considering the short contact distances it is probably on the order of nanosecond time scale though for a more accurate estimation quantum mechanics studies of the tunneling effect between Co(II)Sep molecule and the binding residues are required. Nevertheless, this study is the first of this type on P450 BM3 and, in the limit of the approximation adopted, it provided useful information to further experimental study on mediated electron transfer of this important enzyme. In this sense, our results provide guidelines to the design of novel mutants of the enzyme with a more efficient mediated ET catalysis.

Finally, the presented study evidences how MD simulation is an important tool for a rational process development of electro-enzymatic processes.[70] The more knowledge gained about the process on a molecular level, the more accurate models can be developed, and thereby improved predictions for future designs are possible.

Acknowledgement

Author Information

Corresponding Author:

Prof. Dr. Danilo Roccatano

E-mail: droccatano@lincoln.ac.uk

Current Address: School of Mathematics and Physics, University of Lincoln, Brayford Pool, Lincoln, LN6 7TS, United Kingdom

Associated content

Supporting Information

Tables: GROMOS96 43a1 force field parameters for Co(II)Sep and partial charges on Co(II/III)Sep, backbone-backbone RMSD, Radius of gyrations, average SASA values, ET pathways from 10CoS and 40CoS simulations. Figures: RMSD matrix and cluster analysis,

contact map of CoSep binding on heme domain and P45C$_\alpha$ and A191C$_\alpha$ distance as a function

of time. This information is available free of charge via the Internet at http://pubs.acs.org.

REFERENCES

1.　　　Kohlmann, C.; Markle, W.; Lutz, S., Electroenzymatic synthesis. *J. Mol. Catal. B-Enzym.*
2008, *51*, 57-72.

2.　　　Udit, A. K.; Gray, H. B., Electrochemistry of heme-thiolate proteins. *Biochem. Biophys.*
Res. Commun. **2005,** *338*, 470-476.

3.　　　Luetz, S.; Giver, L.; Lalonde, J., Engineered enzymes for chemical production.
Biotechnol Bioeng **2008,** *101*, 647-653.

4.　　　Prabhulkar, S.; Tian, H.; Wang, X.; Zhu, J. J.; Li, C. Z., Engineered proteins: redox
properties and their applications. *Antioxid. Redox Signal.* **2012,** *17*, 1796-1822.

5.　　　Krieg, T.; Huttmann, S.; Mangold, K.-M.; Schrader, J.; Holtmann, D., Gas diffusion
electrode as novel reaction system for an electro-enzymatic process with chloroperoxidase.
Green Chemistry **2011,** *13*, 2686-2689.

6.　　　Ley, C.; Schewe, H.; Ströhle, F. W.; Ruff, A. J.; Schwaneberg, U.; Schrader, J.;
Holtmann, D., Coupling of electrochemical and optical measurements in a microtiter plate for the
fast development of electro enzymatic processes with P450s. *J. Mol. Catal. B-Enzym.* **2013,** *92*,
71-78.

7.　　　Kochius, S.; Park, J. B.; Ley, C.; Konst, P.; Hollmann, F.; Schrader, J.; Holtmann, D.,
Electrochemical regeneration of oxidised nicotinamide cofactors in a scalable reactor. *J. Mol.*
Catal. B-Enzym. **2014,** *103*, 94-99.

8.   Chefson, A.; Auclair, K., Progress towards the easier use of P450 enzymes. *Mol. Biosyst.* **2006,** *2*, 462-469.

9.   Wong, L. L., Cytochrome P450 monooxygenases. *Curr. Opin. Chem. Biol.* **1998,** *2*, 263-268.

10.   Guengerich, F. P., Common and uncommon cytochrome P450 reactions related to metabolism and chemical toxicity. *Chem. Res. Toxicol.* **2001,** *14*, 611-650.

11.   Shumyantseva, V. V.; Bulko, T. V.; Archakov, A. I., Electrochemical reduction of cytochrome P450 as an approach to the construction of biosensors and bioreactors. *J. Inorg. Biochem.* **2005,** *99*, 1051-1063.

12.   Kumar, S., Engineering cytochrome P450 biocatalysts for biotechnology, medicine and bioremediation. *Expert Opin. Drug Metab. Toxicol.* **2010,** *6*, 115-131.

13.   Schwaneberg, U.; Appel, D.; Schmitt, J.; Schmid, R. D., P450 in biotechnology: zinc driven omega-hydroxylation of p-nitrophenoxydodecanoic acid using P450 BM-3 F87A as a catalyst. *J. Biotechnol.* **2000,** *84*, 249-257.

14.   Davies, T. J.; Brookes, B. A.; Fisher, A. C.; Yunus, K.; Wilkins, S. J.; Greene, P. R.; Wadhawan, J. D.; Compton, R. G., A Computational and Experimental Study of the Cyclic Voltammetry Response of Partially Blocked Electrodes. Part II: Randomly Distributed and Overlapping Blocking Systems. *J. Phy. Chem. B* **2003,** *107*, 6431-6444.

15.   Narhi, L. O.; Fulco, A. J., Characterization of a catalytically self-sufficient 119,000-dalton cytochrome P-450 monooxygenase induced by barbiturates in Bacillus megaterium. *J. Biol. Chem.* **1986,** *261*, 7160-7169.

16.   Narhi, L. O.; Fulco, A. J., Identification and Characterization of 2 Functional Domains in Cytochrome-P-450bm-3, a Catalytically Self-Sufficient Monooxygenase Induced by Barbiturates in Bacillus-Megaterium. *J. Biol. Chem.* **1987,** *262*, 6683-6690.

17.   Whitehouse, C. J. C.; Bell, S. G.; Wong, L.-L., P450BM3 (CYP102A1): connecting the dots. *Chem. Soc. Rev.* **2012,** *41*, 1218-1260.

18.   Peterson, J. A.; Sevrioukova, I.; Truan, G.; GrahamLorence, S. E., P450BM-3: A tale of two domains - Or is it three? *Steroids* **1997,** *62*, 117-123.

19.   Munro, A. W.; Leys, D. G.; McLean, K. J.; Marshall, K. R.; Ost, T. W.; Daff, S.; Miles, C. S.; Chapman, S. K.; Lysek, D. A.; Moser, C. C.; Page, C. C.; Dutton, P. L., P450 BM3: the very model of a modern flavocytochrome. *Trends Biochem. Sci.* **2002,** *27*, 250-257.

20.   Warman, A. J.; Roitel, O.; Neeli, R.; Girvan, H. M.; Seward, H. E.; Murray, S. A.; McLean, K. J.; Joyce, M. G.; Toogood, H.; Holt, R. A.; Leys, D.; Scrutton, N. S.; Munro, A. W., Flavocytochrome P450 BM3: an update on structure and mechanism of a biotechnologically important enzyme. *Biochem. Soc. Trans.* **2005,** *33*, 747-753.

21.   Girvan, H. M.; Waltham, T. N.; Neeli, R.; Collins, H. F.; McLean, K. J.; Scrutton, N. S.; Leys, D.; Munro, A. W., Flavocytochrome P450 BM3 and the origin of CYP102 fusion species. *Biochem. Soc. Trans.* **2006,** *34*, 1173-1177.

22.   Schuhmann, W., Amperometric enzyme biosensors based on optimised electron-transfer pathways and non-manual immobilisation procedures. *J. Biotechnol.* **2002,** *82*, 425-441.

23.   Holtmann, D.; Mangold, K.-M.; Schrader, J., Entrapment of cytochrome P450 BM-3 in polypyrrole for electrochemically-driven biocatalysis. *Biotechnol. Lett.* **2009,** *31*, 765-770.

24.   Nazor, J.; Dannenmann, S.; Adjei, R. O.; Fordjour, Y. B.; Ghampson, I. T.; Blanusa, M.; Roccatano, D.; Schwaneberg, U., Laboratory evolution of P450 BM3 for mediated electron

transfer yielding an activity-improved and reductase-independent variant. *Protein Eng. Des. Sel.* **2008,** *21*, 29-35.

25.   Cekic, S. Z.; Holtmann, D.; Guven, G.; Mangold, K. M.; Schwaneberg, U.; Schrader, J., Mediated electron transfer with P450cin. *Electrochem. Commun.* **2010,** *12*, 1547-1550.

26.   Udit, A. K.; Arnold, F. H.; Gray, H. B., Cobaltocene-mediated catalytic monooxygenation using holo and heme domain cytochrome P450 BM3. *J. Inorg. Biochem.* **2004,** *98*, 1547-1550.

27.   Strohle, F. W.; Cekic, S. Z.; Magnusson, A. O.; Schwaneberg, U.; Roccatano, D.; Schrader, J.; Holtmann, D., A computational protocol to predict suitable redox mediators for substitution of NAD(P)H in P450 monooxygenases. *J. Mol. Catal. B-Enzym.* **2013,** *88*, 47-51.

28.   Roccatano, D.; Wong, T. S.; Schwaneberg, U.; Zacharias, M., Toward understanding the inactivation mechanism of monooxygenase P450 BM-3 by organic cosolvents: a molecular dynamics simulation study. *Biopolymers* **2006,** *83*, 467-476.

29.   Roccatano, D.; Wong, T. S.; Schwaneberg, U.; Zacharias, M., Structural and dynamic properties of cytochrome P450 BM-3 in pure water and in a dimethylsulfoxide/water mixture. *Biopolymers* **2005,** *78*, 259-267.

30.   Verma, R.; Schwaneberg, U.; Roccatano, D., Conformational Dynamics of the FMN-Binding Reductase Domain of Monooxygenase P450BM-3. *J. Chem. Theory Comput.* **2013,** *9*, 96-105.

31.   Verma, R.; Schwaneberg, U.; Roccatano, D., Insight into the redox partner interaction mechanism in cytochrome P450BM-3 using molecular dynamics simulations. *Biopolymers* **2014,** *101*, 197-209.

32.　　van Gunsteren, W. F.; Billeter, S. R.; Eising, A. A.; Hunenberger, P. H.; Kruger, P.; Mark, A. E.; Scott, W. R. P.; Tironi, I. G., Biomolecular Simulation: The GROMOS96 Manual and User Guide. *VdF: Hochschulverlag AG an der ETH Zurich and BIOMOS b.v, Zurich, Groningen.* **1996**.

33.　　Beratan, D. N.; Betts, J. N.; Onuchic, J. N., Protein electron transfer rates set by the bridging secondary and tertiary structure. *Science* **1991,** *252*, 1285-1288.

34.　　Onuchic, J. N.; Beratan, D. N.; Winkler, J. R.; Gray, H. B., Pathway analysis of protein electron-transfer reactions. *Annu. Rev. Biophys. Biomol. Struct.* **1992,** *21*, 349-377.

35.　　Bacchi, A.; Ferranti, F.; Pelizzi, G., Structures of two cobalt(III) sepulchrate complexes. *Acta Crystallogr., Sect. C: Cryst. Struct. Commun.* **1993,** *49*, 1163-1169.

36.　　Dehayes, L. J.; Busch, D. H., Conformational Studies of Metal-Chelates .1. Intra-Ring Strain in 5-Membered and 6-Membered Chelate Rings. *Inorg. Chem.* **1973,** *12*, 1505-1513.

37.　　Becke, A. D., Density-functional thermochemistry. III. The role of exact exchange. *J. Chem. Phys.* **1993,** *98*, 5648-5652.

38.　　Hay, P. J.; Willard, R. W., Ab initio effective core potentials for molecular calculations. Potentials for the transition metal atoms Sc to Hg. *J. Chem. Phys.* **1985,** *82*, 270-283.

39.　　Creaser, I. I.; Harrowfield, J. M.; Herlt, A. J.; Sargeson, A. M.; Springborg, J.; Geue, R. J.; Snow, M. R., Sepulchrate: a macrobicyclic nitrogen cage for metal ions. *J. Am. Chem. Soc.* **1977,** *99*, 3181-3182.

40.　　Breneman, C. M.; Wiberg, K. B., Determining Atom-Centered Monopoles from Molecular Electrostatic Potentials - the Need for High Sampling Density in Formamide Conformational-Analysis. *J. Comput. Chem.* **1990,** *11*, 361-373.

41.   Frisch, M. J.; Trucks, G. W.; Schlegel, H. B.; Scuseria, G. E.; Robb, M. A.; Cheeseman, J. R.; Scalmani, G.; Barone, V.; Mennucci, B.; Petersson, G. A.; Nakatsuji, H.; Caricato, M.; Li, X.; Hratchian, H. P.; Izmaylov, A. F.; Bloino, J.; Zheng, G.; Sonnenberg, J. L.; Hada, M.; Ehara, M.; Toyota, K.; Fukuda, R.; Hasegawa, J.; Ishida, M.; Nakajima, T.; Honda, Y.; Kitao, O.; Nakai, H.; Vreven, T.; Montgomery, J. A.; Peralta, J. E.; Ogliaro, F.; Bearpark, M.; Heyd, J. J.; Brothers, E.; Kudin, K. N.; Staroverov, V. N.; Kobayashi, R.; Normand, J.; Raghavachari, K.; Rendell, A.; Burant, J. C.; Iyengar, S. S.; Tomasi, J.; Cossi, M.; Rega, N.; Millam, J. M.; Klene, M.; Knox, J. E.; Cross, J. B.; Bakken, V.; Adamo, C.; Jaramillo, J.; Gomperts, R.; Stratmann, R. E.; Yazyev, O.; Austin, A. J.; Cammi, R.; Pomelli, C.; Ochterski, J. W.; Martin, R. L.; Morokuma, K.; Zakrzewski, V. G.; Voth, G. A.; Salvador, P.; Dannenberg, J. J.; Dapprich, S.; Daniels, A. D.; Farkas; Foresman, J. B.; Ortiz, J. V.; Cioslowski, J.; Fox, D. J., Gaussian 09, Revision B.01. In *Gaussian 09, Revision B.01, Gaussian, Inc., Wallingford CT*, Wallingford CT, 2009.

42.   Berendsen, H. J. C.; Postma, J. P. M.; van Gunsteren, W. F.; Hermans, J., Interaction models for water in relation to protein hydration. *Intermol. Forces* **1981**, 331-342.

43.   Allen, M. P.; Tidesley, D. J., *Stastistical mechanics: Computer simulations of liquids* Oxford university press: Oxford, England, 1987; p 58-60.

44.   Sevrioukova, I. F.; Li, H. Y.; Zhang, H.; Peterson, J. A.; Poulos, T. L., Structure of a cytochrome P450-redox partner electron-transfer complex. *Proc. Natl. Acad. Sci. U. S. A.* **1999,** *96*, 1863-1868.

45.   Roccatano, D., Structure, dynamics, and function of the monooxygenase P450 BM-3: insights from computer simulations studies. *J. Phys. Condens. Matter* **2015,** *27*, 273102.

46.   Hess, B.; Bekker, H.; Berendsen, H. J. C.; Fraaije, J. G. E. M., LINCS: A linear constraint solver for molecular simulations. *J. Comput. Chem.* **1997,** *18*, 1463-1472.

47.   Miyamoto, S.; Kollman, P. A., Settle - an Analytical Version of the Shake and Rattle Algorithm for Rigid Water Models. *J. Comput. Chem.* **1992,** *13*, 952-962.

48.   Darden, T.; York, D.; Pedersen, L., Particle Mesh Ewald - an N.Log(N) Method for Ewald Sums in Large Systems. *J. Chem. Phys.* **1993,** *98*, 10089-10092.

49.   Berendsen, H. J. C.; Postma, J. P. M.; Vangunsteren, W. F.; Dinola, A.; Haak, J. R., Molecular-Dynamics with Coupling to an External Bath. *J. Chem. Phys.* **1984,** *81*, 3684-3690.

50.   Hess, B.; Kutzner, C.; van der Spoel, D.; Lindahl, E., GROMACS 4: Algorithms for highly efficient, load-balanced, and scalable molecular simulation. *J. Chem. Theory Comput.* **2008,** *4*, 435-447.

51.   Humphrey, W.; Dalke, A.; Schulten, K., VMD: Visual molecular dynamics. *J. Mol. Graphics* **1996,** *14*, 33-&.

52.   Pettersen, E. F.; Goddard, T. D.; Huang, C. C.; Couch, G. S.; Greenblatt, D. M.; Meng, E. C.; Ferrin, T. E., UCSF Chimera--a visualization system for exploratory research and analysis. *J. Comput. Chem.* **2004,** *25*, 1605-1612.

53.   Daura, X.; Gademann, K.; Jaun, B.; Seebach, D.; van Gunsteren, W. F.; Mark, A. E., Peptide folding: When simulation meets experiment. *Angew. Chem. Int. Edit.* **1999,** *38*, 236-240.

54.   Balabin, I. A.; Hu, X.; Beratan, D. N., Exploring biological electron transfer pathway dynamics with the Pathways Plugin for VMD. *J. Comput. Chem.* **2012,** *33*, 906-910.

55.   Marcus, R. A.; Sutin, N., Electron transfers in chemistry and biology. *Biochim. Biophys. Acta* **1985,** *811*, 265-322.

56. Munro, A. W.; Daff, S.; Coggins, J. R.; Lindsay, J. G.; Chapman, S. K., Probing electron transfer in flavocytochrome P-450 BM3 and its component domains. *Eur. J. Biochem.* **1996,** *239*, 403-409.

57. Page, C. C.; Moser, C. C.; Chen, X.; Dutton, P. L., Natural engineering principles of electron tunnelling in biological oxidation-reduction. *Nature* **1999,** *402*, 47-52.

58. Moser, C. C.; Chobot, S. E.; Page, C. C.; Dutton, P. L., Distance metrics for heme protein electron tunneling. *Biochim. Biophys. Acta* **2008,** *1777*, 1032-1037.

59. Paulsen, M. D.; Ornstein, R. L., Dramatic differences in the motions of the mouth of open and closed cytochrome P450 BM-3 by molecular dynamics simulations. *Proteins: Stuct., Func., Bioinf.* **1995,** *21*, 237-243.

60. Shehzad, A. Insights into the Structural Basis for Activity and Selectivity of P450 BM3 Monooxygenase. RWTH Aachen University, Germany, 2013.

61. Chen, C. K.; Shokhireva, T.; Berry, R. E.; Zhang, H.; Walker, F. A., The effect of mutation of F87 on the properties of CYP102A1-CYP4C7 chimeras: altered regiospecificity and substrate selectivity. *J. Biol. Inorg. Chem.* **2008,** *13*, 813-824.

62. Murataliev, M. B.; Trinh, L. N.; Moser, L. V.; Bates, R. B.; Feyereisen, R.; Walker, F. A., Chimeragenesis of the fatty acid binding site of cytochrome P450BM3. Replacement of residues 73-84 with the homologous residues from the insect cytochrome P450 CYP4C7. *Biochemistry* **2004,** *43*, 1771-1780.

63. Lewis, J. C.; Bastian, S.; Bennett, C. S.; Fu, Y.; Mitsuda, Y.; Chen, M. M.; Greenberg, W. A.; Wong, C. H.; Arnold, F. H., Chemoenzymatic elaboration of monosaccharides using engineered cytochrome P450BM3 demethylases. *Proc. Natl. Acad. Sci. U. S. A.* **2009,** *106*, 16550-16555.

64.   Munro, A. W.; Malarkey, K.; McKnight, J.; Thomson, A. J.; Kelly, S. M.; Price, N. C.; Lindsay, J. G.; Coggins, J. R.; Miles, J. S., The role of tryptophan 97 of cytochrome P450 BM3 from Bacillus megaterium in catalytic function. Evidence against the 'covalent switching' hypothesis of P-450 electron transfer. *Biochem. J.* **1994,** *303 (Pt 2)*, 423-428.

65.   Ferrero, V. E.; Andolfi, L.; Di Nardo, G.; Sadeghi, S. J.; Fantuzzi, A.; Cannistraro, S.; Gilardi, G., Protein and electrode engineering for the covalent immobilization of P450 BMP on gold. *Anal. Chem.* **2008,** *80*, 8438-8446.

66.   Rentmeister, A.; Brown, T. R.; Snow, C. D.; Carbone, M. N.; Arnold, F. H., Engineered Bacterial Mimics of Human Drug Metabolizing Enzyme CYP2C9. *Chemcatchem* **2011,** *3*, 1065-1071.

67.   Salazar, O.; Cirino, P. C.; Arnold, F. H., Thermostabilization of a cytochrome p450 peroxygenase. *Chembiochem* **2003,** *4*, 891-893.

68.   Li, H. M.; Mei, L. H.; Urlacher, V. B.; Schmid, R. D., Cytochrome P450 BM-3 evolved by random and saturation mutagenesis as an effective indole-hydroxylating catalyst. *Appl. Biochem. Biotechnol.* **2008,** *144*, 27-36.

69.   Tosstorff, A.; Dennig, A.; Ruff, A. J.; Schwaneberg, U.; Sieber, V.; Mangold, K.-M.; Schrader, J.; Holtmann, D., Mediated electron transfer with monooxygenases—Insight in interactions between reduced mediators and the co-substrate oxygen. *J. Mol. Catal. B-Enzym.* **2014,** *108*, 51-58.

70.   Krieg, T.; Sydow, A.; Schröder, U.; Schrader, J.; Holtmann, D., Reactor concepts for bioelectrochemical syntheses and energy conversion. *Trends Biotechnol.* **2014,** *32*, 645-655.

Table of Contents and Abstract Graphic for Submissions.

$$K_{ET} = \frac{2\pi}{\hbar} \frac{e^{\frac{-(\Delta G + \lambda)^2}{4\lambda k_B T}}}{\sqrt{4\pi\lambda k_B T}} |T_{DA}|^2$$